Desalination 408 (2017) 13–24

Contents lists available at ScienceDirect

Desalination

journal homepage: www.elsevier.com/locate/desal

Recycling brine water of reverse osmosis desalination employing adsorption desalination: A theoretical simulation

Ehab S. Ali [a], Ahmed S. Alsaman [b], K. Harby [c], Ahmed A. Askalany [b,*], Mohamed Refaat Diab [c], Sobhy M. Ebrahim Yakoot [d,e]

[a] Holding Company for Water and Waste Water in Sohag, 82524, Egypt
[b] Mechanical Engineering Dept., Faculty of Industrial Education, Sohag University, Sohag 82524, Egypt
[c] Mechanical Power Engineering and Energy Dept., Faculty of Engineering, Minia University, Minia 61511, Egypt
[d] Biochemistry Dep., Prince Mutaib Chair for Biomarkers of Osteoporosis, College of Science, King Saud University, PO Box 2455, Riyadh 11451, Saudi Arabia
[e] Atomic Energy Authority, Hot Laboratories Centre, 13759, Egypt

HIGHLIGHTS

- An innovative combination between RO and AD desalination systems has been proposed.
- RO brine is recycled by employing adsorption desalination.
- The proposed system has been studied theoretically by using a MATALB code.

ARTICLE INFO

Article history:
Received 19 July 2016
Received in revised form 4 December 2016
Accepted 4 December 2016
Available online 8 January 2017

Keywords:
Reverse osmosis
Adsorption
Desalination
Cooling

ABSTRACT

Intake, pretreatment and brine disposal cost of reverse osmosis sea water desalination systems represent about 25% of total cost of the desalinated water. The present study investigates effect of reverse osmosis brine recycling employing adsorption desalination on overall system desalinated water recovery. The adsorption desalination produces dual useful effects which are high quality potable water and cooling effect. Reverse osmosis desalination is simulated by engineering equation solver (EES). The brine leaving reverse osmosis system is fed to adsorption desalination system. The adsorption desalination is driven by a low temperature heat source such as solar energy. The adsorption desalination system has been simulated by MATLAB. Results show that the proposed combination system recovery increases and permeate salinity decreases. In addition to system performance improvements, a cooling effect is generated and can be utilized for cooling applications.

Nomenclature

A	area (m^2)
A_m	membrane area (m^2)
Cp	specific heat (kJ/kg·k)
D_s	coefficient of surface diffusion (m^2/s)
D_{so}	pre-exponential coefficient (m^2/s)
E	characteristic energy (kJ/kg)
E_a	activation energy (kJ/kg)
h_{fg}	water latent heat (kJ/kg)
H_{st}	isosteric heat of adsorption (kJ/kg)
k_s	salt permeability (kg/m^2 s ppm)
k_w	water permeability (kg/m^2 s kPa)
M	mass (kg)
m	mass flow rate (kg/s)
$\overline{m}$	average mass flow rate (kg/s)
P	pressure (kPa)
Q	heat energy (kJ/s)
R	permeate recovery, dimensionless
$\bar{R}$	universal gas constant (kJ/kg·k)
R_p	average radius of the particle (m)
SR	salt rejection, dimensionless
T	temperature (°C)
t	time (s)
U	overall heat transfer coefficient (w/m^2·k)
X	concentration (ppm)
$X_{average}$	average salinity in the feed compartment (ppm)
τ	number of cycle per day (–)
ΔP	pressure drop through RO membrane (kPa)
$\Delta\pi$	osmotic pressure drop through RO membrane (kPa)
π	osmotic pressure (kPa)

* Corresponding author.
E-mail address: ahmed_askalany3@yahoo.com (A.A. Askalany).

http://dx.doi.org/10.1016/j.desal.2016.12.002
0011-9164/

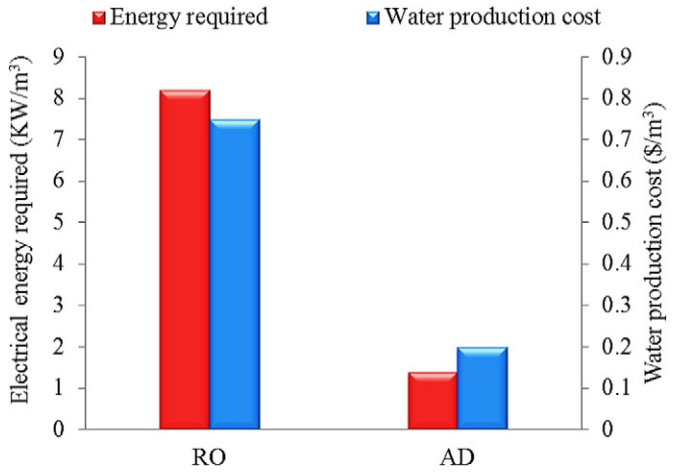

Fig. 1. The electrical energy and cost required for desalinated water for RO and AD systems [22,23].

ω	adsorption capacity (kg/kg)
ω_o	maximum adsorption capacity (kg/kg)

Subscripts

ads	adsorption
b	brine
ch	chilled water
cond	condenser
des	desorption
evap	evaporator
f	feed
hex	heat exchanger
hw	heating water
i	reverse osmosis module no in pressure vessel
in	inlet
out	outlet
p	permeate
s	salt
sat	saturation
sg	silica gel
sur	surrounding
sw	sea water
v	vapor
w	water

1. Introduction

Rapid growth of reverse osmosis (RO) desalination system is because it has the ability of producing desalinated water with a relatively low cost [1]. RO desalination system consists of four major components: pretreatment, high pressure pump, RO membrane modules assembly and post-treatments (permeate post-treatment and brine disposal) [2]. Intake, pretreatment and brine disposal cost of RO sea water desalination system represent about 25% of total cost [3,4].

The adsorption desalination system (ADS) is being developed steadily over the past decades and is considered one of the possible alternatives to traditional desalination systems to overcome their problems [5,6]. This technology depends on employing adsorbent materials such as silica gel. The ADS mimics the evaporation in the ambient by low temperature solar collectors and condensing water vapor at high altitude producing pure water with no need for fossil fuel. Evaporation of the seawater occurs at low-temperatures between 5 °C and 20 °C [7].

Unlike the conventional methods, adsorption technology is driven by low-grade heat such as waste heat or solar energy [6,8]. Also, ADS has few moving parts. The ADS has the ability to treat or desalinate seawater and brackish water which contain organic compounds [9]. In addition to these advantages, the ADSs produce cooling water which could reduce the dependency on the conventional electric driven cooling systems contributing to global warming with high-energy consumption.

A hybrid of Multi Effect desalination (MED) with ADS has been studied by Thu et al. [5]. AD-MED water production rate was increased to about two folds with comparing to a traditional MED while the gain output ratio (GOR) and the performance ratio (PR) had been increased by 40% [5].

Thu et al. [10] reported a hybrid AD-MED system with different numbers of effects compared to conventional MED systems. The simulation showed that the increase of AD-MED system performance is more effective at lower top brine temperature.

Shahzad et al. [11] reported that hybrid of AD-MED system could increase the desalinated water to about three folds with same top brine temperature comparing to conventional MED systems.

Thu et al. [12] proposed a hybrid AD-MED system utilizing low heat source temperature. The evaporation ensued at low temperatures ranging from 35 °C to 7 °C. This proposed cycle provided a significant high performance ratio. The specific water production, PR and GOR were about 1.0 m^3/h ton of silica gel, 6.3 and 5.1, respectively. Thu et al. [13] investigated three beds two evaporators ADS. In the proposed system, COP had been increased to about 0.82 at longer cycle time.

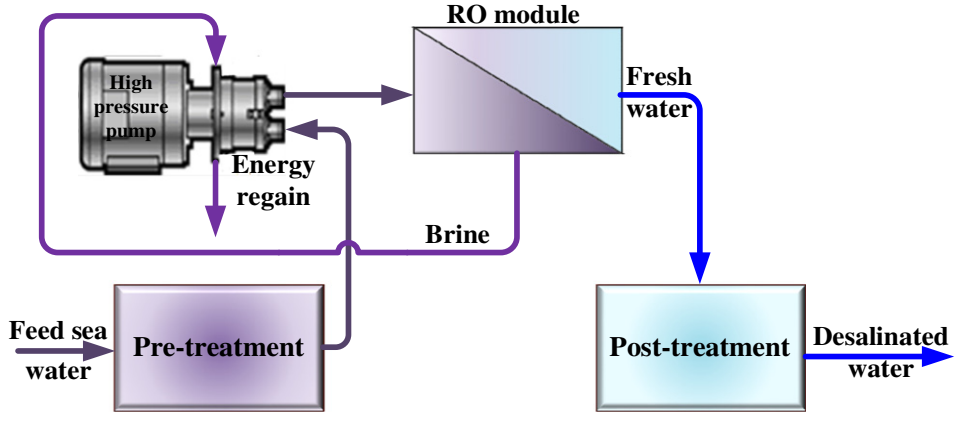

Fig. 2. RO system components.

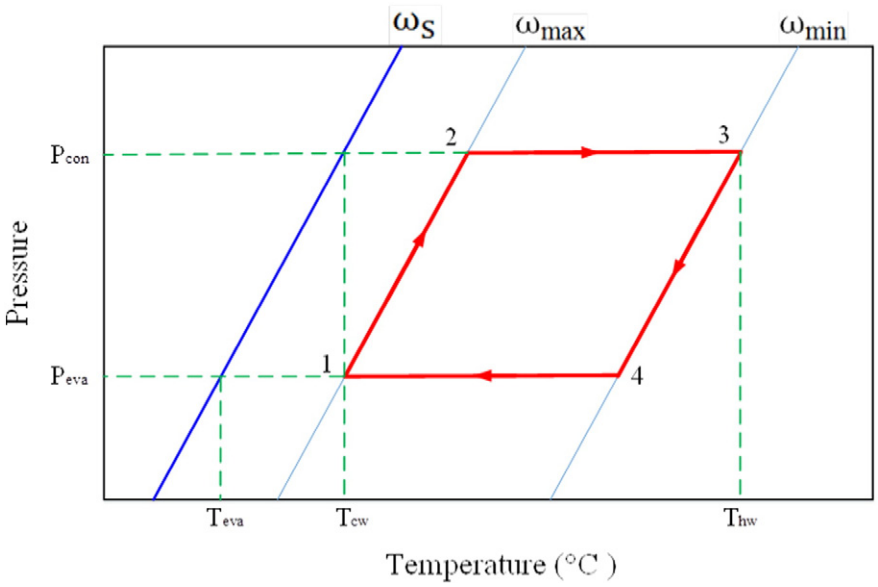

Fig. 3. P-T-ω diagram of the ideal AD cycle (1 → 2 isosteric heating, 2 → 3 desorption, 3 → 4 isosteric cooling, 4 → 1 adsorption).

Askalany [14] investigated theoretically a hybrid mechanical vapor compression with the ADS. The water production of proposed system increases by about 10–45% with comparing to ADS alone.

Performance of hybrid RO desalination system, multi-stage flash (MSF) and electro dialysis (ED) systems were also studied by Thampy et al. [15]. He presented a hybrid ED-RO system for increasing water recovery of brackish water. It was noted that the energy consumption for investigated system was from 8 to10 kWh/m^3 of desalinated water with 50 to 60% recovery.

A1-Bahri et al. [16] studied the hybrid RO plant operation and MSF optimum seawater feed temperature. It had been noted that a little advantage for feed water preheating before the RO system. Marcovecchio et al. [17] investigated theoretically a model of a hybrid MSF-RO system. The investigated system was aimed to determine the optimal design operating conditions.

Helal et al. [18–20] presented a study of a hybrid MSF-RO system. This investigated study consisted of three parts: (i) modelling, problem definition and algorithm in which, the description and cost

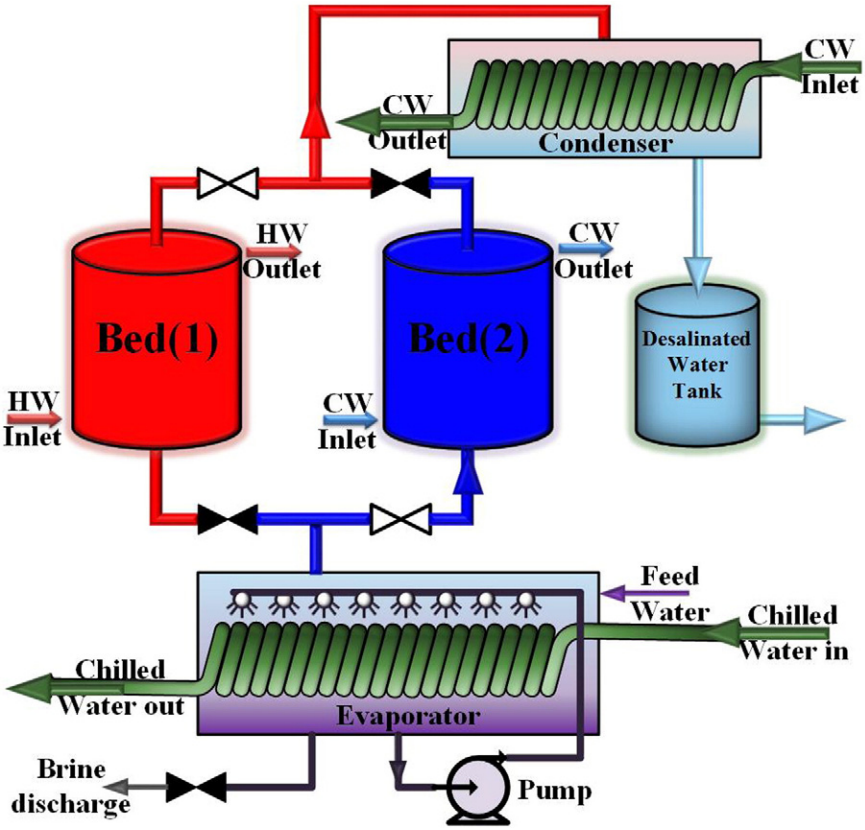

Fig. 4. ADS components [6].

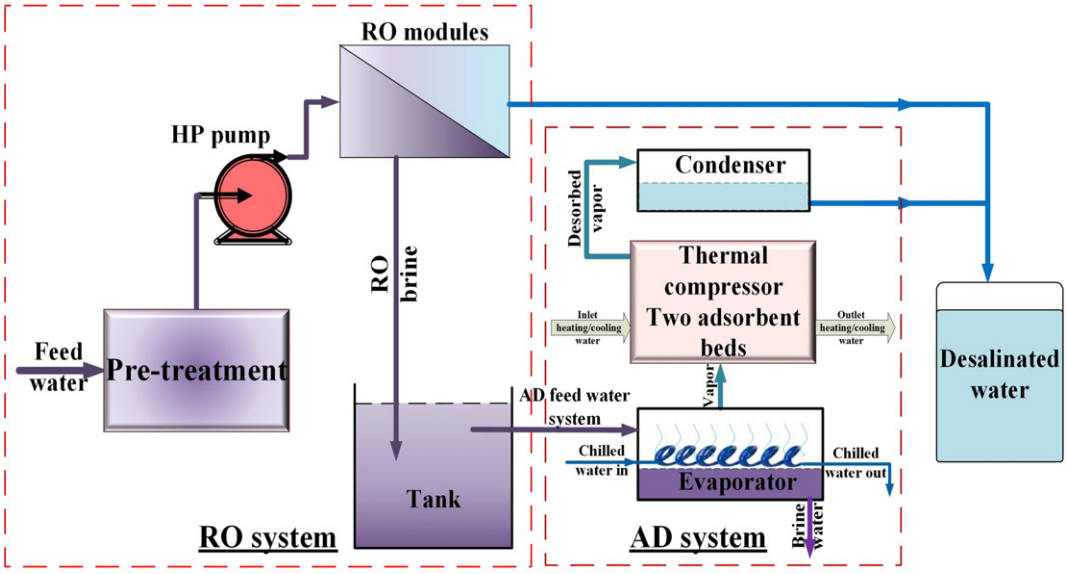

Fig. 5. Schematic of the investigated RO-AD system.

analysis were presented. (ii) Discussion and presentation of the optimal designs obtained and water costs; and (iii) discussion of sensitivity analysis.

Cardona et al. [21] presented the design of optimization tri-functional power-MSF-RO system. The optimal design of the tri-functional cogeneration was based on profit maximization and exergo-economics.

Fig. 1 shows the electrical energy and cost required for production one cubic permeate of desalinated water for RO system and ADS [22–23].

This study presents RO brine recycling effect employing ADS on the required sea water feed flow rate for the same desalinated water and consequently, on the cost of desalinated water.

2. Physical model

2.1. Reverse osmosis

Main feature of the RO desalination system is its simplicity with relativity low energy consumption. RO system components are illustrated in Fig. 2 [24]. RO desalination system is an assembly of modules which are connected in a certain pattern in RO pressure vessel. For simplicity, RO pressure vessel contains four RO modules SWRHLE-440i type. The performance of RO membrane is validated with RO System Analysis (ROSA) software which its results are considered as experimental results [25,26].

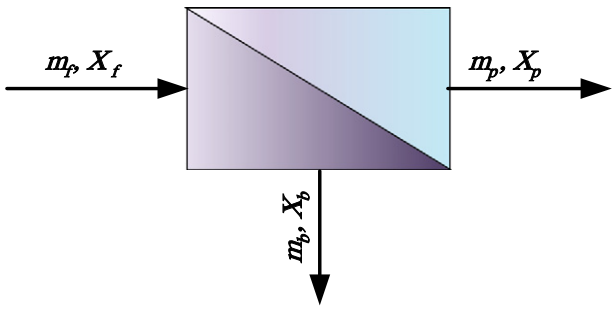

Fig. 6. One module of RO modules arrangements.

2.2. Adsorption desalination cycle

Adsorption desalination cycle consists of four processes as following:

1) Isosteric heating process: adsorbent material is heated up without changing its concentration which stays constant at the maximum concentration(ω_{max}).
2) Desorption process: adsorbent material is heated and its concentration changes from ω_{max} to the minimum concentration(ω_{min}). This heat called the heat of desorption (Q_{des}). At the same time, the released vapor is turned to liquid phase in the condenser at the condensation temperature(T_{cond}).
3) Isosteric cooling process: adsorbent material is cooled down without changing the concentration which stays constant at ω_{min}.

Table 1
The design and operating conditions [22,23,33].

Symbol	Description	Value	Unit
A_{bed}	Adsorbent bed heat transfer area	2.46 [32]	m^2
A_{con}	Condenser heat transfer area	3.73 [32]	m^2
A_{eva}	Evaporator heat transfer area	1.91 [32]	m^2
Cp_{al}	Aluminum specific heat	905 [32]	J/kg·k
Cp_{cu}	Cupper specific heat	386 [32]	J/kg·k
Cp_{ch}	Chilled water specific heat	4200	J/kg k
Cp_{v}	Water specific heat vapor phase	1890	J/kg k
Cp_{w}	Water specific heat liquid phase	4180	J/kg k
Cp_{sg}	Silica gel specific heat	921 [22]	J/kg·k
D_{so}	Diffusion coefficient	2.54×10^{-4} [22]	m^2/s
E_a	Activation energy	4.2×10^4 [22]	J/kg
H_{st}	Heat of adsorption	2.37×10^6 [33]	J/kg
$\dot{m}_w$	Cooling/heating water flow rate	1.3 [32]	kg/s
$\dot{m}_{ch}$	Chilled water flow rate	0.7 [32]	kg/s
M_{Al}	Bed heat exchanger fin weight(Al)	51.2 [32]	kg
M_{con}	Condenser heat exchanger tube weight(Cu)	27.28 [32]	kg
M_{cu}	Bed heat exchanger tube weight(Cu)	64.04 [32]	kg
M_{eva}	Evaporator heat exchanger tube weight(Cu)	12.45 [32]	kg
M_{sg}	Weight of silica gel in each bed	47 [32]	kg
$M_{w,eva}$	Liquid water in side evaporator initially	50 [32]	kg
R_p	Average radius of silica gel particle	1.7×10^{-4} [22]	m
$T_{ch,in}$	Chilled water inlet temperature	14	°C
T_{cw}	Cooling source temperature	30	°C
T_{hw}	Heating source temperature	85	°C
t_{cycle}	Cycle time	900	s
U_{bed}	Heat transfer coefficient of bed	1724.14 [32]	$W/m^2 \cdot k$
U_{con}	Condenser heat transfer coefficient	4115.23 [32]	$W/m^2 \cdot k$
U_{eva}	Evaporator heat transfer coefficient	2557.54 [32]	$W/m^2 \cdot k$

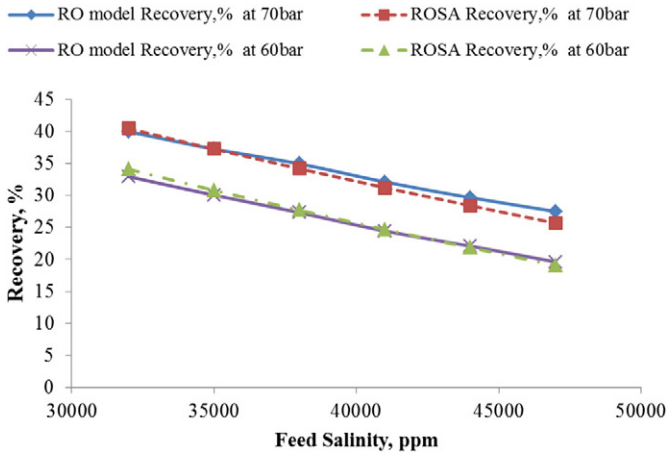

Fig. 7. RO permeate recovery with changing seawater feed salinity for the cases of 60 and 70 bar feed pressure.

4) Isobaric adsorption process: adsorbent material adsorbs vapor at P_{evap}. The concentration increases from ω_{min} to ω_{max} and releasing the heat of adsorption.

Fig. 3 illustrates the ideal AD cycle and Fig. 4 shows the ADS. It consists of three main parts, two adsorbent beds, condenser and evaporator as illustrated in Fig. 4. Desorption and adsorption processes are running in bed (1) and bed (2) respectively. These processes are alternatively in bed (1) and bed (2) every half cycle time [6].

The brine leaving the RO modules is fed to the ADS as shown in Fig. 5. An open air water storage tank must be added after energy recovery devise of the RO system. This tank is used for solving the problem of high RO brine pressure to feed AD evaporator and the problem of intermittent duty of AD feed water intake.

The volume of the adsorbent material for ADS can be estimated by dividing brine flow in cubic meter per day of RO plant by the average of SDWP.

3. Mathematical model

3.1. Mathematical model for RO system

The computations are based on constant feed flow rate and 25 °C temperature of seawater. Fig. 6 illustrates one module of RO system.

Osmotic pressure can be estimated by [27].

$$\pi = 0.07584\, X_f \tag{1}$$

Performance of RO system is evaluated by recovery and salt rejection which are estimated as [28];

$$R = \left(\frac{m_p}{m_f}\right) \times 100 \tag{2}$$

$$SR = \left\{1 - \left(\frac{X_p}{X_f}\right)\right\} \times 100 \tag{3}$$

Mass and salt balances for RO system;

$$m_f = m_p + m_b \tag{4}$$

Average concentration factor is calculated by [25];

$$m_f X_f = m_p X_p + m_b X_b \tag{5}$$

$$X_{fc} = X_f \frac{Ln\left(\frac{1}{1-R_i}\right)}{R_i} \tag{6}$$

It has been noted that a slight pressure drop in feed pressure is occurred when feed water passes through the reverse osmosis element in pressure vessel. The pressure drop can be calculated by [26];

$$Pcd = 0.01\, n\, q_{cave}^{1.7} \tag{7}$$

$$q_{cave} = \frac{m_f + m_b}{2} \tag{8}$$

Experimentally, the concentration polarization factor in membrane is estimated from the following [25];

$$CP = EXP(0.7\, R_i) \tag{9}$$

The following equation estimates the permeate flow rate through RO membrane module [25].

$$m_p = \left(P_f - \frac{P_{cd}}{2} - P_p - \pi_{cave} + \pi_P\right) k_w A_m \tag{10}$$

π_P and π_{cave} are osmotic permeate pressure and average feed side

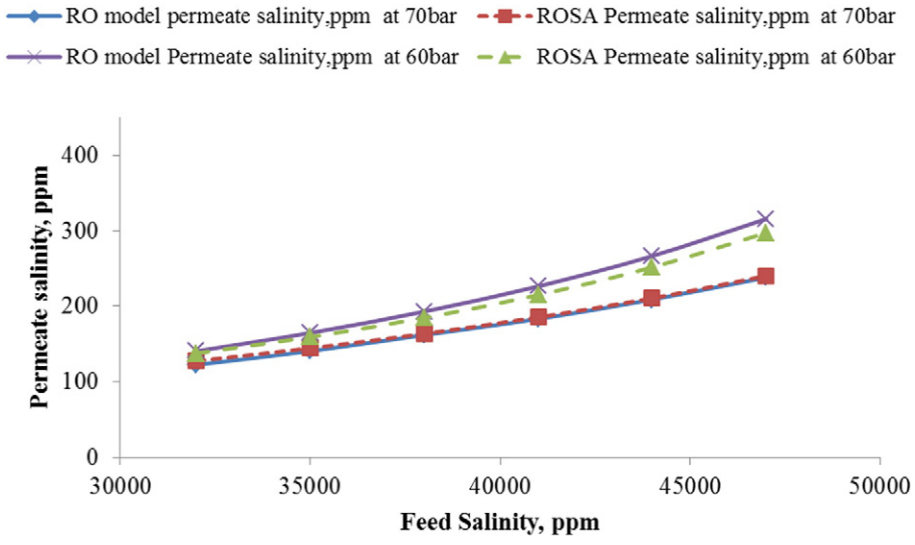

Fig. 8. RO permeate salinity with changing seawater feed salinity for the cases of 60 and 70 bar feed pressure.

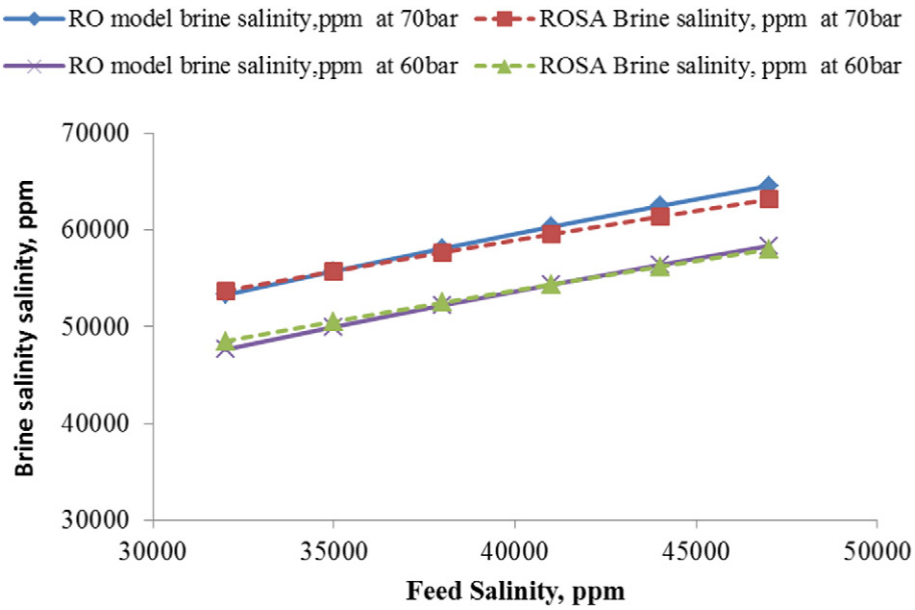

Fig. 9. RO brine discharge salinity with changing seawater feed salinity for the cases of 60 and 70 bar feed pressure.

osmotic pressure which can be calculated from;

$$\pi_P = \pi_f(1-SR) \tag{11}$$

$$\pi_{cave} = \pi_f\, CP\, \frac{X_{fc}}{X_f} \tag{12}$$

The following equation defines permeate concentration [25].

$$X_P = \frac{K_s CP\, X_{fc}\, SR\, A_m}{m_p} \tag{13}$$

3.2. Mathematical model for ADS

3.2.1. Assumptions

The study aimed to estimate the performance of investigated model to the following constraints:

1) The amount of adsorbed vapor, pressure and temperature are uniform through adsorption bed.
2) Heat loss to the environment is neglected as adsorption beds are considered well insulated.
3) Thermal resistance between adsorbent bed and metal tube is neglected.
4) Pipeline water flow resistance is neglected.
5) Properties of adsorbate vapor, metal tube and fluids are constant.
6) The maximum brine concentration is 110,000 ppm [22] and exceeds to 220,000 ppm for salts production purpose as it has proven that the water quality of AD process is independent of high feed salinity (up to 220,000 ppm) inside the evaporator even at high recovery ratio [9].

3.2.2. Characteristics of adsorbent material

In order to estimate the amount of adsorbate uptake by adsorbent material at different pressure, adsorption isotherms should be estimated. Also, adsorption kinetics should be estimated. Modified Freundlich model is used to predicted adsorption isotherms with the constants [29].

$$\omega_o = A(T_{ads})\left\{\frac{P_{sat}(T_{ref})}{P_{sat}(T_{ads})}\right\}^{B(T_{ads})} \tag{14}$$

$$A(T_{ads}) = A_0 + A_1 ioT_{ads} + A_2 T_{ads}^2 + A_3 T_{ads}^3 \tag{15}$$

$$B(T_{ads}) = B_0 + B_1 T_{ads} + B_2 T_{ads}^2 + B_3 T_{ads}^3 \tag{16}$$

3.2.3. Adsorption kinetics

Linear driving force kinetic (LDF) equation is used for estimating transient water vapor uptake [30]:

$$\frac{d\omega}{dt} = k_s a_v(\omega_o - \omega) \tag{17}$$

Where,

$$k_s a_v = 15\frac{D_s}{R_p^{\,2}} \tag{18}$$

$$D_s = D_{so}\, exp\left\{-\frac{E_a}{\bar{R}T}\right\} \tag{19}$$

3.2.4. Mass balance

The mass balance of ADS is estimated by;

$$\frac{dM_{sw,evap}}{dt} = \theta \dot{m}_{sw,in} - \gamma \dot{m}_b - n\left(\frac{d\omega_{ads}}{dt}\right)M_{sg} \tag{20}$$

$$M_{sw,eva}\frac{dX_{sw,eva}}{dt} = \theta X_{sw,in}\dot{m}_{sw,in} - \gamma X_{sw,in}\dot{m}_b - n.X_D\left(\frac{d\omega_{ads}}{dt}\right)M_{sg} \tag{21}$$

The values of the coefficients θ, γ and n for different operation modes are stated in [31].

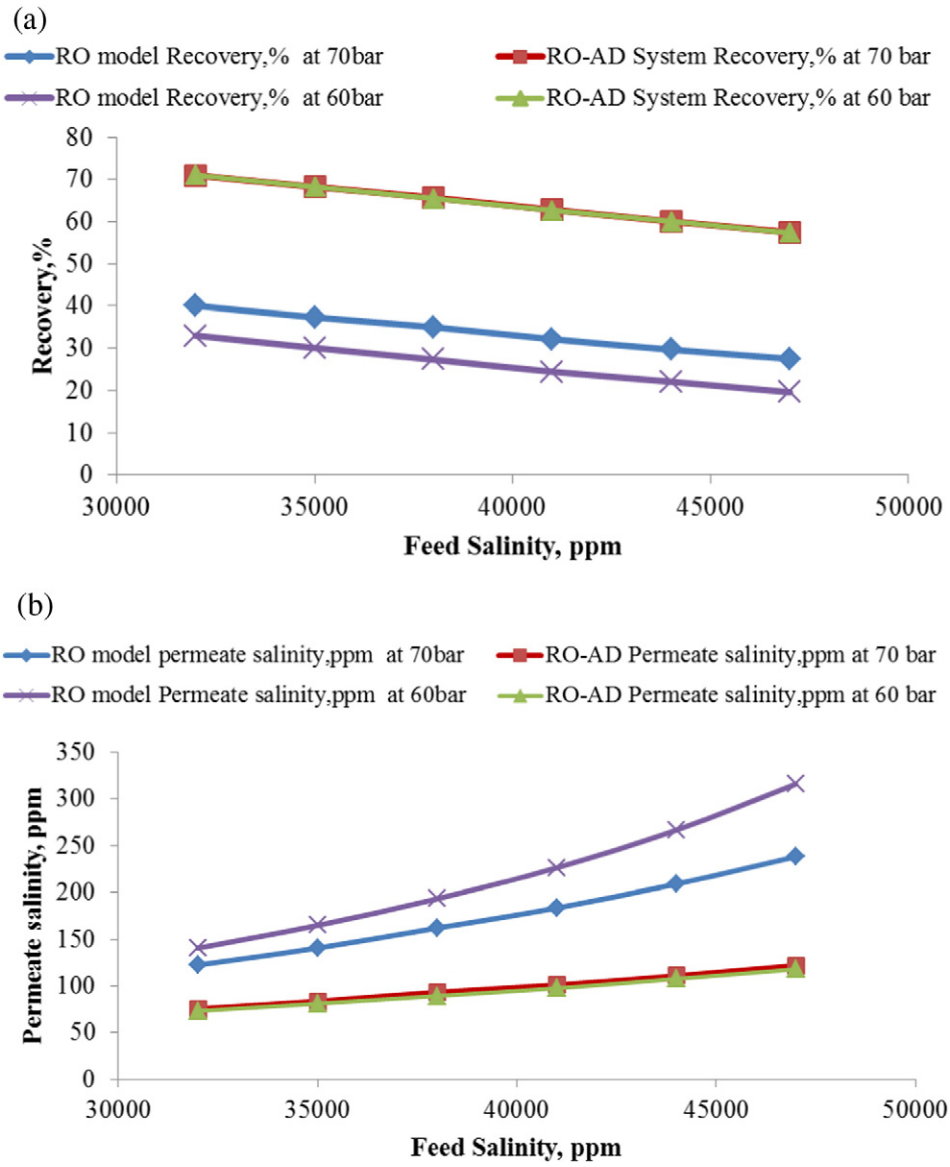

Fig. 10. RO-AD permeate parameters with changing seawater feed salinity for the cases of 60 and 70 bar feed pressure. (a) Recovery. (b) Permeate salinity.

3.2.5. Energy balance equations

3.2.5.1. Energy balance for the bed. Energy balance for the adsorbent bed can be expressed by;

$$\left[\left(M_{sg}c_{p_{sg}} + M_{sg}c_{p_v}\omega\right) + \left(M_{bed}c_{p\,bed}\right)\right]\frac{dT_{bed}}{dt} = M_{sg}H_{st}\frac{d\omega_{bed}}{dt} - \dot{m_w}c_{p_w}\left(T_{w,out} - T_{w,in}\right) \quad (22)$$

The outlet water temperature from each heat exchanger can be calculated using LMTD method.

$$T_{w,out} = T_{bed} + \left(T_{w,in} - T_{bed}\right)\ exp\left\{\frac{-\left(U_{bed}A_{bed}\right)}{\left(\dot{m_w}c_{p_w}\right)}\right\} \quad (23)$$

3.2.5.2. Energy balance for the condenser. The heat balance of the condenser can be given as;

$$\left(M_{w,cond}c_{p_w} + M_{hex,c}c_{p\,hex,c}\right)\frac{dT_{cond}}{dt} = h_f\left(T_{cond}\right)\frac{dM_d}{dt} + n.h_{fg}\left(T_{cond}\right)\frac{d\omega_{des}}{dt}M_{sg} + \dot{m_w}c_{p_w}\left(T_{cond}\right)\left(T_{w,in} - T_{w,out}\right)^{cond}\dot{m_b} \quad (24)$$

M_d is distillated water mass extracted from the condenser. The first term in the right hand side stands for sensible heat by outlet desalinated water, the second term stands for latent heat generated by vapor condensation and the third term stand for heat absorbed by cooling water.

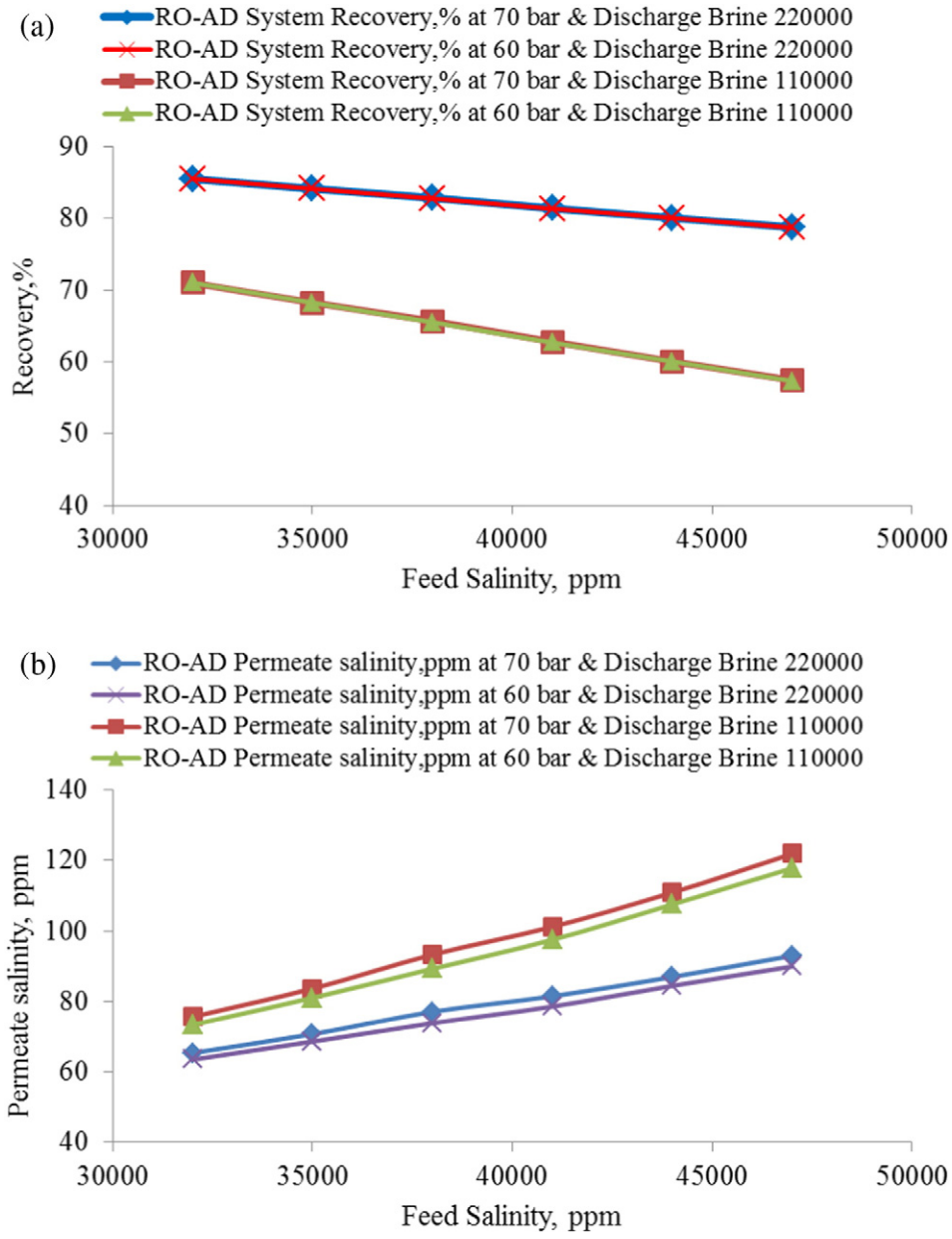

Fig. 11. RO-AD permeate parameters with changing seawater feed salinity at 60 and 70 bar feed pressure for cases 110,000 and 220,000 ppm brine concentration limit. (a) Recovery. (b) Permeate salinity.

3.2.5.3. Energy balance for the evaporator. The evaporator energy balance is expressed as;

$$\left(M_{sw,eva}c_{p_s}(T_{eva},X_{sw,eva})+M_{cu,eva}c_{p_{cu,eva}}\right)\frac{dT_{eva}}{dt} = \theta h_f(T_{eva},X_{sw,eva})\dot{m}_{s,in}-n.h_{fg}(T_{eva})\frac{d\omega_{des}}{dt}M_{sg} + \dot{m}_{ch}c_{p_{ch}}(T_{ch,in}-T_{ch,out})-\gamma h_f(T_{eva},X_{s,eva})\dot{m}_b \quad (25)$$

The effect of feed concentration is taken into consideration in the previous equation of heat balance for evaporator. Seawater specific heat and enthalpy are estimated as functions of pressure, temperature and salinity. The concentrated salt water causes vapor pressure depression as known as boiling point elevation (BPE). As a result of this, the water vapour uptake is reduced as it is mainly depends on temperature and pressure [22].

The heat of evaporation, desorption and condensation are estimated by;

$$Q_{evap}=\int_0^{t_{cycle}}\dot{m}_{ch}C_p(T_{evap})(T_{ch,in}-T_{ch,out}) \quad (26)$$

$$Q_{des}=\int_0^{t_{cycle}}\dot{m}_{hw}C_p(T_{hw,in}-T_{hw,out}) \quad (27)$$

$$Q_{cond}=\int_0^{t_{cycle}}\dot{m}_{cond}C_p(T_{cond})(T_{cond,out}-T_{cond,in}) \quad (28)$$

3.2.6. Cycle performance parameters

The cycle is analyzed using key performance parameters: specific daily water production (SDWP), specific cooling power (SCP) and the

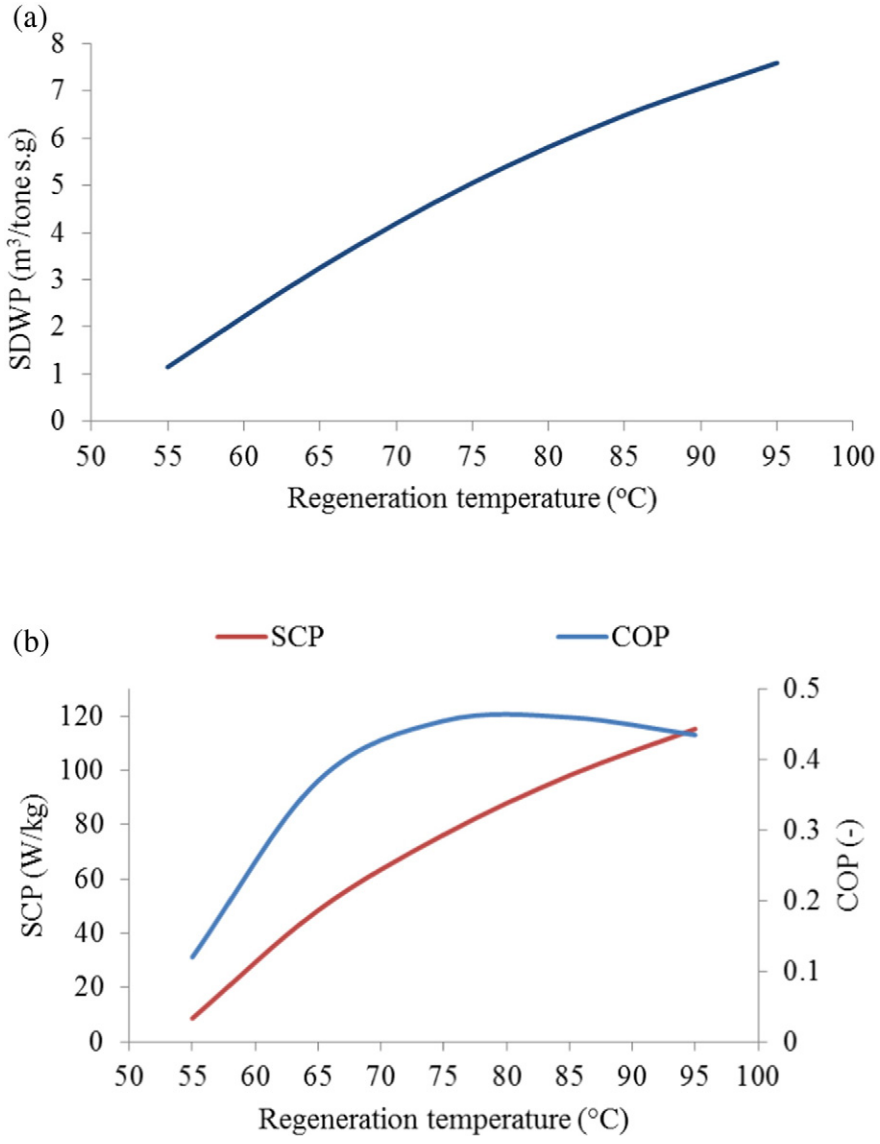

Fig. 12. AD performance parameters with changing generation temperature (a) SDWP, (b) COP and SCP.

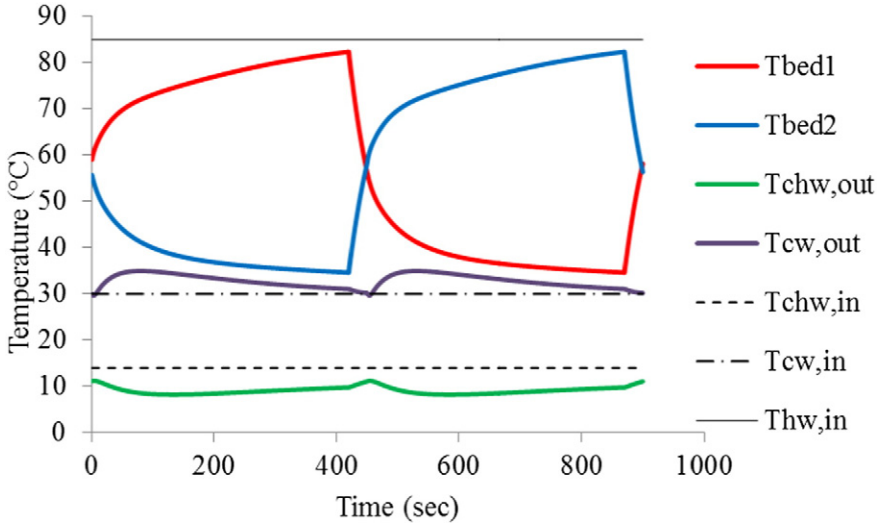

Fig. 13. AD temperature profiles for rated conditions.

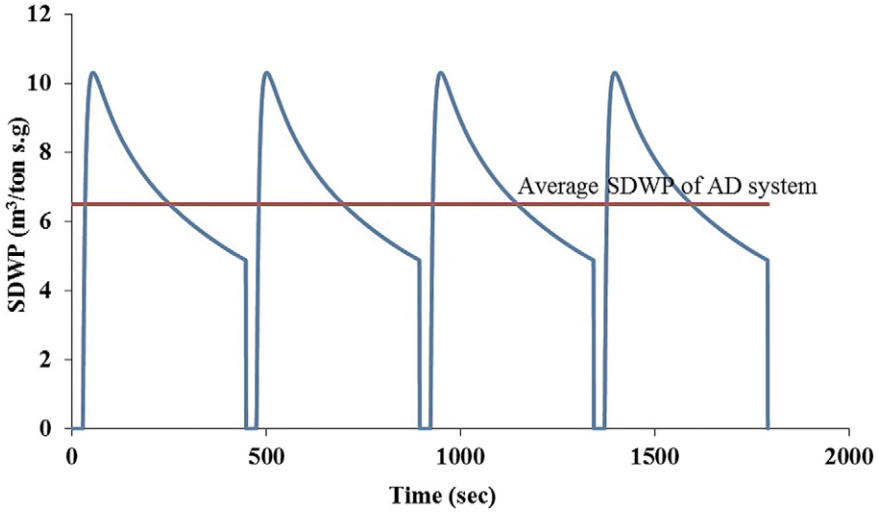

Fig. 14. The average SDWP for investigated ADS at 85 °C regeneration temperature.

coefficient of performance (COP) as following;

$$SDWP = \int_0^{t_{cycle}} \frac{Q_{cond}\tau}{h_{fg}M_{sg}}dt \quad (29)$$

$$SCP = \frac{Q_{evap}}{M_{sg}} \quad (30)$$

$$COP = \frac{Q_{evap}}{Q_{des}} \quad (31)$$

Electrical power consumptions for water pumps are neglected. The values of the designing and operating conditions are shown in Table 1 [22,32,33].

3.3. RO-AD system recovery

The investigated ADS has an intermittent effect of desalinated water in contrary the RO system has a continued production rate. So that water storage tank for RO brine (AD feed) has been added to solve the problem of intermittent duty of AD intake as illustrated in Fig. 5. This open air tank must be added after energy recovery devise for RO system.

Applying mass and salt balance;

$$\dot{m}_{b,RO} = \overline{m}_{p,AD} + \overline{m}_{b,AD} \quad (32)$$

$$X_{b,RO}\dot{m}_{b,RO} = X_{p,AD}\overline{m}_{p,AD} + X_{b,AD}\overline{m}_{b,AD} \quad (33)$$

ADS recovery is given by;

$$R_{AD} = \frac{\overline{m}_{p,AD}}{\dot{m}_{b,RO}} \quad (34)$$

The overall system recovery is given by Eq. (35);

$$R_{overall\ system} = \frac{\overline{m}_{p,AD} + \dot{m}_{p,RO}}{\dot{m}_f} \quad (35)$$

EES is used for solve RO model while MATLAB is used to solve the ADS and the combination between the AD and RO.

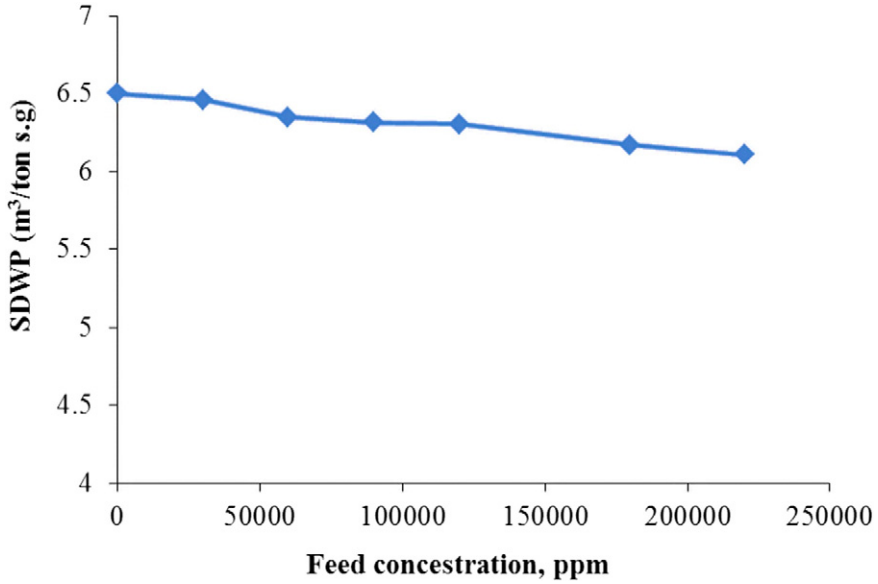

Fig. 15. The effect of feed water concentration on SDWP of ADS.

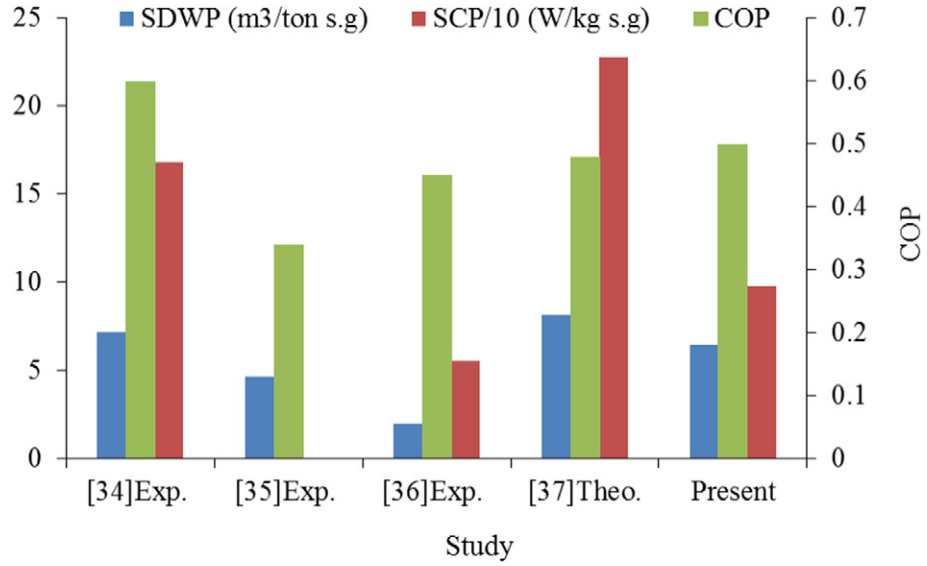

Fig. 16. A comparing between previous studies [34–37] and present study for AD system.

4. Results and discussion

The present study illustrates effect of the RO brine recycling employing AD system. RO desalination permeate is affected by different parameters such as feed salinity, feed pressure, material (cellulose triacetate and polyamide) and membrane construction (spiral wound and hollow fine).

This paper shows the effects of these parameters on the proposed ROAD system. Seawater salinity is taken from 30,000 ppm to 45,000 ppm. These salinities include the range of salinities of Red and Mediterranean seas. Fig. 7 shows RO recovery that decreases with increasing feed salinity. The figure also illustrates the RO recovery at 60 and 70 bar feed pressure. The simulation model has been compared with ROSA at different seawater feed salinity. As indicated from Fig. 7, there is a good agreement, more than 95%, between RO model and ROSA software for RO system recovery.

Fig. 8 shows that the RO permeate salinity increases with increasing the feed salinity. The figure also illustrates permeate salinity at 60 and 70 bar feed pressure. As indicated from Fig. 8, there is a good agreement, more than 94%, between RO model and ROSA software for permeate salinity.

Fig. 9 shows that RO brine discharge salinity increases with increasing feed salinity. The figure also illustrates RO brine discharge salinity at 60 and 70 bar feed pressure.

RO brine discharge is fed to AD system. Fig. 10(a) shows that ROAD recovery (desalinated mass flow rate to seawater mass flow rate) compared to RO recovery with different seawater feed salinity for cases of 60 and 70 bar feed pressure. The results indicate that ROAD recovery is higher than the RO recover by about 20%. The results indicate that ROAD recovery increases with decreasing seawater feed salinity.

As shown from Fig. 10(b) the ROAD permeate salinity for 60 and 70 bar is nearly equivalent as the AD system permeate salinity is about 15 ppm. Therefore, it reduces the difference between 60 and 70 bar seawater feed pressure cases. Also, the ROAD overall recovery for cases 60 and 70 bar seawater feed pressure is nearly equivalent.

In case of salt production purposes, the brine concentration limit exceeded a high limit of 220,000 ppm and the ROAD system permeate parameters could be changed. It has been proven that the water quality of AD process is independent of high feed salinity (up to 220,000 ppm) inside the evaporator even at high recovery ratio [9]. The discharged brine can be fed directly to concentrator for salt extraction.

Fig. 11 shows results for permeate parameters at 110,000 and 220,000 ppm brine concentration for RO-AD. Fig. 11(a) indicates that RO-AD recovery increases about 15% in the case of 220,000 ppm brine concentration limit compared to the case of 110,000 ppm brine concentration limit. Also, the permeate salinity is decreased as shown in Fig. 11(b).

Fig. 12 shows the results for AD performance (SDWP - COP - SCP) for different generation temperature. Fig. 12(a) indicates that SDWP increases with increasing generation temperature. Fig. 12(b) illustrates the COP and SCP with generation temperature. COP curve has one peak point between 80 and 90 °C. The AD system can be operated by low temperature heat source as solar energy.

Fig. 13 illustrates the AD temperature profiles for two beds, outlet condenser cooling water and outlet chilled water. After during the steady state condition, the average of outlet chilled water temperature is about 9 °C for the rated operating conditions.

The investigated AD system could produce about 6.5 m^3 desalinated water per ton of silica gel daily at 85 °C regeneration temperature as illustrated in Fig. 14. Fig. 15 illustrates that SDWP decreases with the increase of feed water concentration. As stated in [9,33] and reported in the figure, the AD system has the ability for desalinating the water with high feed water concentration up to 220,000 ppm.

Fig. 16 illustrates a comparing between previous studies [34–37] and the present model for ADS. The figure shows that the present model for ADS has good agreements with the previous experimental study.

5. Conclusion

In this study, an innovative combination between RO and AD desalination systems has been proposed. The proposed system has been studied theoretically and the mathematical model is solved using a MATLAB code. The main advantage of the ROAD is it increases the system recovery with low potential permeate salinity. Also, the silica gel–water AD system can be driven effectively by low-temperature heat source between 55 and 95 °C which could be easily offered by solar or waste energy. RO simulation model is compared with ROSA software assuming that ROSA results are the baseline experiment. It was found that there is a good agreement, more than 95%, between RO model and ROSA software. The results for RO-AD indicate that the system recovery increased by about 25% compared to a single stage RO system. The RO-AD system has a SCP of 100 W/kg.sg with a COP of 0.46.

In case of salt production the brine concentration is about 220,000 ppm. In this case the permeate recovery increased by about 15% compared to the case of 110,000 ppm brine salinity concentration. The discharged brine can be fed directly to concentrator or crystallizer for salt extraction.

Acknowledgments

This project was supported by King Saud University, Deanship of Scientific Research, College of Science Research Center.

References

[1] Y.Y. Lu, Optimum design of RO system under different feed concentration and product specification, J. Membr. Sci. 287 (2007) 219–229.
[2] B. Djebedjian, RO desalination plant in Nuweiba city (case study), IWTC11Sharm El-Sheikh, Egypt, Conference Proceedings 2007, pp. 315–330.
[3] M. Gökçek, Ö.B. Gökçek, Technical and economic evaluation of freshwater production from a wind-powered small-scale seawater reverse osmosis system (WP-SWRO), Desalination 381 (2016) 47–57.
[4] Water-use Association Desalination, Seawater desalination costs:1–19, https://www.watereuse.org/wp-content/uploads/2015/10/WateReuse_Desal_Cost_White_Paper.pdf (accessed 15.02.2016).
[5] K. Thu, Y. Kim, G. Amy, W. Chun, K. Ng, A hybrid multi-effect distillation and adsorption cycle, Appl. Energy 104 (2013) 810–821.
[6] A.S. Alsaman, A.A. Askalany, K. Harby, M.S. Ahmed, A state of the art of hybrid adsorption desalination–cooling systems, Renew. Sust. Energ. Rev. 58 (2016) 692–703.
[7] K. Thu, A. Chakraborty, Y. Kim, A. Myat, B. Saha, Numerical simulation and performance investigation of an advanced adsorption desalination cycle, Desalination 308 (2013) 209–218.
[8] B.B. Saha, H. Khairul, I.I. El-Sharkawy, K. Shigeru, Adsorption characteristics and heat of adsorption measurements of R-134a on activated carbon, Int. J. Refrig. 32 (7) (2009) 1563–1569.
[9] Y.-D. Kim, K. Thu, M.E. Masry, K.C. Ng, Water quality assessment of solar-assisted adsorption desalination cycle, Desalination 344 (2014) 144–151.
[10] K. Thu, Y.-D. Kim, G. Amy, W. Chun, K. Ng, A synergetic hybridization of adsorption cycle with the multi-effect distillation (MED), Appl. Therm. Eng. 62 (2014) 245–255.
[11] M.W. Shahzad, K.C. Ng, K. Thu, B. Saha, W.G. Chun, Multi effect desalination and adsorption desalination (MED-AD): a hybrid desalination method, Appl. Therm. Eng. 72 (2) (2014) 289–297.
[12] K. Thu, Y.-D. Kim, M.W. Shahzad, J. Saththasivam, K.C. Ng, Performance investigation of an advanced multi-effect adsorption desalination (MEAD) cycle, Appl. Therm. Eng. 159 (2015) 469–477.
[13] K. Thu, B.B. Saha, K.J. Chua, K.C. Ng, Performance investigation of a waste heat-driven 3-bed 2-evaporator adsorption cycle for cooling and desalination, Int. J. Heat Mass Transf. (101) (2016) 1111–1122.
[14] A.A. Askalany, Innovative mechanical vapor compression adsorption desalination (MVC-AD) system, Appl. Therm. Eng. 106 (2016) 286–292.
[15] S. Thampy, G.R. Desale, V.K. Shahi, B.S. Makwana, P.K. Ghosh, Development of hybrid electrodialysis-reverse osmosis domestic desalination unit for high recovery of product water, Desalination 282 (2011) 104–108.
[16] Z.K. Al-Bahri, W.T. Hanbury, T. Hodgkiess, Optimum feed temperatures for seawater reverse osmosis plant operation in an MSF/SWRO hybrid plant, Desalination 138 (2001) 335–339.
[17] M.G. Marcovecchio, S.F. Mussati, P.A. Aguirre, J.N. Scenna, Optimization of hybrid desalination processes including multi stage flash and reverse osmosis systems, Desalination 182 (2005) 111–122.
[18] A.M. Helal, A.M. El-Nashar, E. Al-Katheeri, S. Al-Malek, Optimal design of hybrid RO/MSF desalination plants Part I: modeling and algorithms, Desalination 154 (2003) 43–66.
[19] A.M. Helal, A.M. El-Nashar, E. Al-Katheeri, S. Al-Malek, Optimal design of hybrid RO/MSF desalination plants Part II: results and discussion, Desalination 160 (2004) 13–27.
[20] A.M. Helal, A.M. El-Nashar, E. Al-Katheeri, S. Al-Malek, Optimal design of hybrid RO/MSF desalination plants Part III: sensitivity analysis, Desalination 169 (2004) 43–60.
[21] E. Cardona, A. Piacentino, Optimal design of cogeneration plants for seawater desalination, Desalination 166 (2004) 411–426.
[22] K. Thu, Adsorption desalination theory and experimentsPhD thesis National University of Singapore, Singapore, 2010.
[23] K. Thu, A. Chakraborty, B.B. Saha, W.G. Chun, K.C. Ng, Life-cycle cost analysis of adsorption cycles for desalination, Desalin. Water Treat. 20 (2010) 1–10.
[24] M.S. Atab, A.J. Smallbone, A.P. Roskilly, An operational and economic study of a reverse osmosis desalination system for potable water and land irrigation, Desalination 397 (2016) 174–184.
[25] A. Altaee, Computational model for estimating reverse osmosis system design and performance: part-one binary feed solution, Desalination 291 (2012) 101–105.
[26] A. Altaee, Theoretical study on feed water designs to reverse osmosis pressure vessel, Desalination 326 (2013) 1–9.
[27] T. El-Dessouky, M. Ettouney, Fundamentals of salt water desalination, Chapter 7 Reverse Osmosis, first ed.Elsevier, 2002.
[28] T. Kaghazchi, M. Mehri, M.T. Ravanchi, A. Kargari, A mathematical modeling of two industrial seawater desalination plants in the Persian Gulf region, Desalination 252 (2010) 135–142.
[29] A. Rezk, R. Al-Dadah, S. Mahmoud, A. Elsayed, Characterisation of metal organic frameworks for adsorption cooling, Int. J. Heat Mass Transf. 55 (2012) 7366–7374.
[30] K. Habib, B. Choudhury, P.K. Chatterjee, B.B. Saha, Study on a solar heat driven dual mode adsorption chiller, Energy 63 (2013) 133–141.
[31] K.C. Ng, K. Thu, Y. Kim, A. Chakraborty, G. Amy, Adsorption desalination: an emerging low-cost thermal desalination method, Desalination 308 (2013) 161–179.
[32] C.Y. Tso, C. CYH, S.C. Fu, Performance analysis of a waste heat driven activated carbon based composite adsorbent-water adsorption chiller using simulation model, Int. J. Heat Mass Transf. 55 (2012) 7596–7610.
[33] K.C. Ng, H.T. Chua, C.Y. Chung, C.H. Loke, T. Kashiwagi, A. Akisawa, B.B. Saha, Experimental investigation of the silica gel-water adsorption isotherm characteristics, Appl. Therm. Eng. 21 (2001) 1631–1642.
[34] K. Ng, K. Thu, A. Chakraborty, B. Saha, W. Chun, Solar-assisted dual effect adsorption cycle for the production of cooling effect and potable water, Int. J. Low Carbon Technol. 4 (2) (2009) 61–67.
[35] X. Wang, K. Ng, Experimental investigation of an adsorption desalination plant using low-temperature waste heat, Appl. Therm. Eng. 25 (2005) 2780–2789.
[36] S. Mitra, K. Srinivasan, P. Kumar, S.S. Murthy, P. Dutta, Solar driven adsorption desalination system, Energy Procedia 49 (2014) 2261–2269.
[37] P. Youssef, R. AL-Dadah, S. Mahmoud, H. Dakkama, A. Elsayed, Effect of evaporator and condenser temperatures on the performance of adsorption desalination cooling cycle, Energy Procedia 75 (2015) 1464–1469.